# NJC

Accepted Manuscript

ROYAL SOCIETY OF CHEMISTRY

www.rsc.org/njc

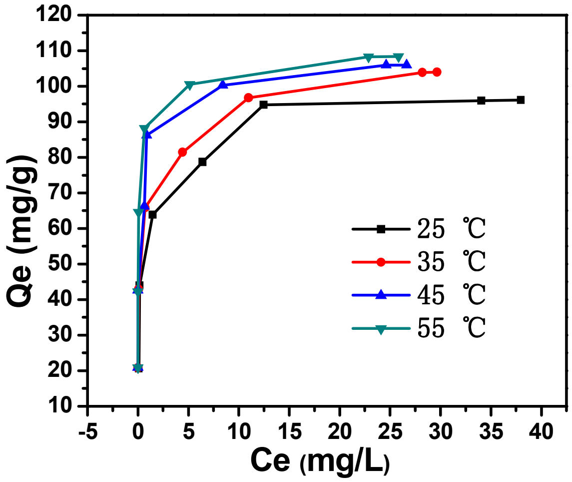
Qe (mg/g)
Ce (mg/L)
120
110
100
90
80
70
60
50
40
30
20
10
-5
0
5
10
15
20
25
30
35
40
25 ℃
35 ℃
45 ℃
55 ℃

New Journal of Chemistry

Dynamic Article Links ►

Cite this: DOI: 10.1039/c0xx00000x

www.rsc.org/xxxxxx

ARTICLE TYPE

# Synthesis of Manganese dioxide/iron oxide/graphene magnetic nanocomposite for enhanced uranium (VI) removal

**Lichao Tan,[a] Jun Wang,*[a, c] Qi Liu,*[a] Yanbo Sun,*[b] Xiaoyan Jing,[a] Lianhe Liu,[c] Jingyuan Liu[a] and Dalei Song[a]**

***Received (in XXX, XXX) Xth XXXXXXXXX 20XX, Accepted Xth XXXXXXXXX 20XX***

**DOI: 10.1039/b000000x**

In this study, we have developed a facile route for the fabrication of manganese dioxide/iron oxide/reduced graphite oxide magnetic nanocomposite ($MnO_2/Fe_3O_4$/rGO). The as-obtained nanomaterial ($MnO_2/Fe_3O_4$/rGO) was characterized by transmission electron microscopy, Fourier-transform infrared spectroscopy, X-ray diffraction, Vibrating sample magnetometry, and Brunauer-Emmett-Teller surface area measurement. $MnO_2/Fe_3O_4$/rGO composite shows extraordinary adsorption capacity and fast adsorption rates for removal of uranium (VI) in aqueous solution. The influence of conditions including dosage of $MnO_2/Fe_3O_4$/rGO composite, pH of aqueous solution, and temperature were investigated. The thermodynamic parameters, including Gibbs free energy ($\Delta G°$), standard enthalpy change ($\Delta H°$) and standard entropy change ($\Delta S°$) for the process, were calculated using the Langmuir constants. The results show that a pseudo-second -order kinetics model can be used to describe the uptake process by a kinetics test. Our present study suggests that $MnO_2/Fe_3O_4$/rGO composite can be used as a potential adsorbent for sorption of uranium (VI) as well as providing a simple, fast separation method for removal of uranium (VI) ions from aqueous solution.

## Introduction

The presence of a high amount of various heavy metals in effluents is known to be detrimental to human health and the environment.[1] Among these heavy metal species, uranium is one of the most dangerous for the environment because of its chemical toxicity and radioactivity. Excessive amounts of uranium have entered into the environment through activities associated with the nuclear industry.[2] Thus, the removal, recovery, and purification of uranium are especially important.

Up to now, several methods, such as chemical precipitation, solvent extraction, membrane separation, and adsorption,[3-9] have been extensively applied for the removal of uranium (VI) from aqueous solutions. Among them, adsorption is considered as an attractive method for the removal of heavy metals. However, biosorbents often cause potential secondary pollution in extreme conditions, have weak mechanical strength, are not easily separated, and are not sufficiently effective. Thus, developing new materials with simple synthesis, high adsorption capacity, easy separation, and good stability in extreme conditions, is highly desired.[10]

Graphene, a rapidly rising star, has been the focus of world attention in energy storage fields owing to its ultrahigh surface area, outstanding electrical conductivity and strong mechanical stability, which makes graphene an attractive candidate as a novel nanoscale building block for adsorption treatment of polluted water.[11] However, to the best of our knowledge, graphene is hydrophobic and usually suffers from irreversible agglomeration in water due to the strong van der Waals interactions between neighboring sheets, which leads to a great loss of effective surface area and consequently a lower adsorption capacity than expected.[12-13] To prevent the restacking of graphene nanosheets, many studies have recently focused on the intercalation of inorganic nanoparticles (e.g. ZnO,[14] $Fe_3O_4$,[15] $CoFe_2O_4$,[16] $MnO_2$,[17] $SiO_2$,[18] $Cu_2O$[19]) into the graphene interlayers.

In the past few years, manganese dioxide ($MnO_2$) is the most important scavenger of aqueous trace metals in soil, sediments, and rocks because of its apparent dominant adsorptive behavior. Compared with iron or aluminum oxides, $MnO_2$ has higher affinities and provides an efficient scavenging pathway for many heavy metals. Nevertheless, manganese oxide coated onto media surfaces using low-cost and simple methods may provide effective surfaces for the removal of heavy metals from wastewater, thereby having promising commercial potential.

Magnetic adsorbents have emerged as a new generation of materials for environmental decontamination since magnetic separation simply involves applying an external magnetic field to extract the adsorbents.[20-24] Iron oxide nanoparticles in the crystalline form of magnetite ($Fe_3O_4$), with low toxicity and supermagnetic and ferromagnetic properties, have attracted extensive interest for numerous applications in various fields, such as magnetic recording media, giant magnetoresistive sensors, photonic crystals, and biomedical applications.[25] Decorating magnetic iron oxide nanoparticles on graphene will impart desirable magnetic properties into the graphene, making the composite promising for a variety of fields such as adsorption, magnetic energy storage, magnetic fluids, catalysis, and environmental remediation.[26-27]

Taking the above factors into account in our study, $MnO_2/Fe_3O_4$/rGO was prepared using a simple method. The as-obtained nanocomposite exhibits the following advantages: first, it can be used for effective adsorption of uranium (VI) ions; second, the adsorbent can be removed completely from aqueous solutions by an external magnetic field; third, regeneration of the adsorbent can be achieved by simply washing with HCl, and the removal efficiency of uranium (VI) was still over 85% after reusing four times.

## Experimental

### Synthesis of the $MnO_2/Fe_3O_4$/rGO nanocomposite

The graphene oxide (GO) was obtained according to the previous report.[28] The synthesized GO was dispersed in water to get a brown dispersion. Exfoliated graphite oxide was obtained by ultrasound (about 0.5 wt. % GO dispersion), using a Sonifier (KQ-500DB, 250 W). Then 0.6 g glucose was completely dissolved in 300 mL of exfoliated graphite oxide solution (0.5 wt. %) and continuously stirred for 30 min at room temperature. Then, 3 mL ammonia solution (25% w/w) was added to the resulting dispersion. After vigorously shaking for a few minutes, the mixture was stirred for 60 min at 95 $^{o}$C. The product was then filtered and washed with distilled water, and was named as rGO. Finally, the obtained rGO was dispersed into 300 mL water for further use.

In a typical synthesis, the as-prepared rGO (0.5 g) was exfoliated by ultrasonication in 80 mL of ethylene glycol (EG) for more than 3 h. 1.6 g $FeCl_3 \cdot 6H_2O$ and 3.2 g sodium acetate (NaAc) were then dissolved in rGO and EG solution at ambient temperature. After stirring for about 30 min, the solution was transferred into a 100 mL Teflon-lined stainless-steel autoclave and kept at 200 $^{o}$C for 6 h and cooled to ambient temperature naturally. The black precipitate was centrifuged, washed with ethanol several times, and finally dried at 60 $^{o}$C in a vacuum oven.

$MnO_2$ was coated onto $Fe_3O_4$/rGO by simple immersion of the $Fe_3O_4$/rGO into a $KMnO_4$ aqueous solution.[29] First, 200 mL of 0.1 M $KMnO_4$ solution was heated to 75 °C for 3 h using a circulator. Subsequently, 1.0 g of $Fe_3O_4$/rGO was added to the solution at pH 5. The temperature of the solution was maintained at 75 °C for 3 h during synthesis. The suspension was filtered and washed several times using deionized water and absolute ethanol, and then dried at 80 °C for 12 h. These materials were denoted as $MnO_2/Fe_3O_4$/rGO.

### Adsorption experiments

A batch technique was applied to study the sorption of uranium (VI) complex from the prepared solutions by $MnO_2/Fe_3O_4$/rGO. Batch sorption experiments were carried out in a thermostated shaker bath. Typically, $MnO_2/Fe_3O_4$/rGO was dispersed in 20 mL solution containing various initial uranium concentrations at different pH values and contact times. The pH was adjusted by adding 0.5 M $HNO_3$ and NaOH into the solution for each experiment. After the adsorption equilibrium, $MnO_2/Fe_3O_4$/rGO was separated from the solution by magnetic separation, and the effluent was analyzed using a Bruker 820-MS ICP-MS instrument. The adsorption capacity $Q_e$ (mg g$^{-1}$) and the % removal of uranium were calculated according to Eqs. (1) and (2):

$$Q_e = (C_0 - C_e) \cdot V / m \quad (1)$$

$$\mathrm{Removal}(\%) = 100 \times (C_0 - C_e) / C_0 \quad (2)$$

where $C_0$ (mg L$^{-1}$) is the uranium (VI) ion concentration in the initial solution, $C_e$ (mg L$^{-1}$) is the equilibrium concentration of uranium (VI) ion in the supernatant, $V$ (L) is the volume of the testing solution and $m$ is the weight of sorbent (g). The error bars indicate the standard deviation estimated from triplicate experiments.

### Characterization

X-ray diffraction (XRD) analysis was performed on a Rigaku D/max-IIIB diffractometer with Cu-Ka irradiation (k =1.54178 Å) with the X-ray source operated at 40 KV and 150 mA. Fourier-transform infrared (FT-IR) spectrum was recorded with an AVATAR 360 FT-IR spectrophotometer using a standard KBr pellets. The magnetic hysteresis loops of samples were measured by a vibrating sample magnetometer (VSM, Lanzhou University LakeShore 7304). $N_2$ adsorption/desorption isotherms were measured at liquid nitrogen temperature (-196 $^{o}$C) using a Micromeritics ASAP 2010 instrument. The surface areas were calculated using the Brunauer–Emmett–Teller (BET) method. Zeta Potential was measured using a Malvern Instrument ZetaSizer Nano ZS90. The morphologies of the samples were characterized using a transmission electron microscope (TEM, FEI Tecnai G2 S-Twin).

### Desorption and regeneration

The recovery of the adsorbent is an important factor in designing an adsorption procedure. To estimate the reversibility of uranium (VI) sorption, desorption experiments using different concentrations of HCl solution were performed. After magnetic separation, the remaining uranium (VI) concentration in the supernatant was measured to evaluate the desorption percentage. The regenerated $MnO_2/Fe_3O_4$/rGO was washed thoroughly with distilled water and then used for the next sorption–desorption cycle.

## Results and discussions

The as-obtained nanomaterial ($MnO_2/Fe_3O_4$/rGO) was characterized by transmission electron microscopy, Fourier-transform infrared spectroscopy, X-ray diffraction, Vibrating sample magnetometry, and Brunauer-Emmett-Teller surface area measurement. The influence of conditions including dosage of $MnO_2/Fe_3O_4$/rGO composite, pH of aqueous solution, Zeta Potential and temperature were investigated.

### Characterization of samples

The crystalline structure of the $Fe_3O_4$/rGO and $MnO_2/Fe_3O_4$/rGO was corroborated by XRD measurements. As seen in Figure 1, the pattern of the $Fe_3O_4$/rGO displays obvious diffraction peaks of $Fe_3O_4$, and the peak positions and relative intensities match well with standard XRD data for the magnetite (JCPDS card, file No. 19-0629). The diffraction peak at 2θ = 24.16° is assigned to the (002) plane of the graphite derived from the short-range order in stacked graphene sheets.[30] The XRD pattern of $MnO_2/Fe_3O_4$/rGO exhibits a new peak at the angles 2θ = 37.64°, which belong to the $MnO_2$ (131).[31] Meanwhile, the XRD pattern of $MnO_2/Fe_3O_4$/rGO exhibits few well-defined peaks involving crystal $MnO_2$, These results suggest that the $MnO_2$ is at a non-stoichiometric and amorphous phase.[32]

The detailed characterization of GO, $Fe_3O_4$/rGO and $MnO_2/Fe_3O_4$/rGO using FTIR analysis techniques are compared in Figure 2. For GO, as indicated by the characteristic peaks at 3414 and 1619 $cm^{-1}$ of the stretching vibrations of $\nu$(OH) and $\nu$(C=O*)* of the carboxylic groups(COOH), respectively. A band at 1385 $cm^{-1}$ should be assigned to C-H. $Fe_3O_4$/rGO shows an additional broad band at 576 $cm^{-1}$, related to the stretching vibration of Fe–O–Fe, characteristic of $Fe_3O_4$. A comparison of GO and $Fe_3O_4$/rGO FTIR spectra, the band at 1619 $cm^{-1}$ shifts to 1666 $cm^{-1}$ and it is evidence of the band of $Fe_3O_4$ spectra due to acetate on the surface. For $MnO_2/Fe_3O_4$/rGO, a broad band is observed in the composite at the low-frequency region of around 624 $cm^{-1}$. The presence of this band is attributed to the Mn–O, Mn–O–Mn, and Fe–O–Fe vibrations.[33]

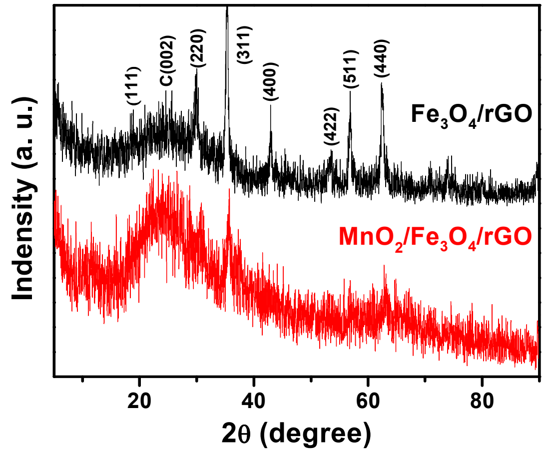

**Figure 1.** XRD patterns of $Fe_3O_4$/rGO and $MnO_2/Fe_3O_4$/rGO.

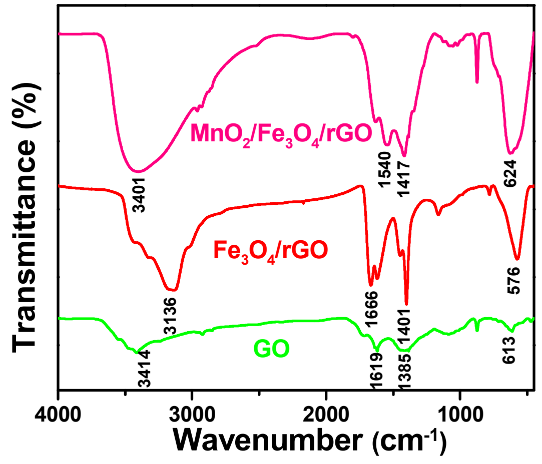

**Figure 2.** FTIR transmission spectra of GO, $Fe_3O_4$/rGO and $MnO_2/Fe_3O_4$/rGO.

The morphology of the rGO, $Fe_3O_4$/rGO and $MnO_2/Fe_3O_4$/rGO were examined by TEM, as shown in Figure 3. Figure 3a shows the image of rGO and Figure 3b shows the image of the $Fe_3O_4$/rGO nanoparticles. rGO has been coated with spherical iron oxide particles which are often aggregated by virtue of their magnetic nature. Figure 3c and 3d show the morphology of the $MnO_2/Fe_3O_4$/rGO. The $Fe_3O_4$/rGO is fully coated with $MnO_2$ and forms a very thin, uniform, and continuous coated layer of $MnO_2$. The HRTEM images in Figure 3e and 3f show a clear lattice between the adjacent fringes. The inter-planar spacing of $MnO_2$ nanoflake is measured to be 0.67 nm, which is in good agreement with literature report of ~0.7 nm for birnessite-type $MnO_2$.[34] The lattice d-spacings of 0.29 nm corresponding to (220) planes of $Fe_3O_4$,[35] is identified in Figure 3f. These characteristics may promote the adsorption process.

The magnetic properties of $Fe_3O_4$/rGO and $MnO_2/Fe_3O_4$/rGO are shown in Figure 4. Their saturation magnetization of 62.4 emu $g^{-1}$ and 13.9 emu $g^{-1}$ is observed for $Fe_3O_4$/rGO and $MnO_2/Fe_3O_4$/rGO, respectively. The reduced saturation magnetization of $MnO_2/Fe_3O_4$/rGO (13.9 emu $g^{-1}$) compared with $Fe_3O_4$/rGO (62.4 emu $g^{-1}$) is ascribed to the presence of diamagnetic $MnO_2$ coating onto $Fe_3O_4$/rGO. In addition, the negligible coercivity or remanence indicates that the two samples exhibit superparamagnetic behaviour. However, its maximum saturation magnetization (13.9 emu $g^{-1}$) is enough to maintain their magnetic recovery performance.[36] These results show that $MnO_2/Fe_3O_4$/rGO composite possesses magnetic responsivity and is easily separated during sorption experiments.

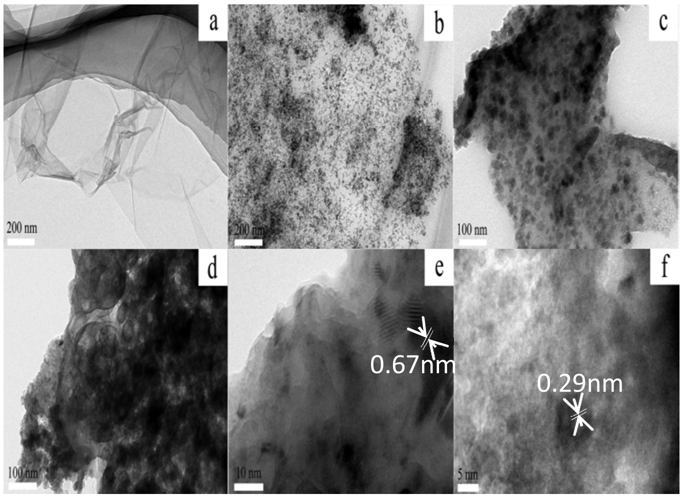

**Figure 3.** Representative TEM images of rGO (a), $Fe_3O_4$/rGO (b) and $MnO_2/Fe_3O_4$/rGO (c and d). HRTEM of $MnO_2/Fe_3O_4$/rGO (e and f).

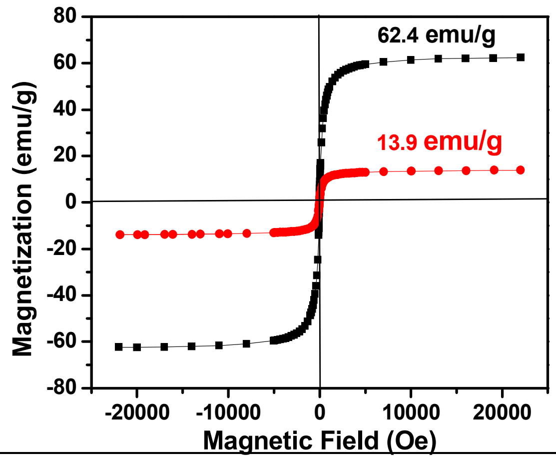

**Figure 4.** Magnetic hysteresis curves for $Fe_3O_4$/rGO and $MnO_2/Fe_3O_4$/rGO.

The physical properties of $Fe_3O_4$/rGO and $MnO_2/Fe_3O_4$/rGO are listed in Table 1. The surface area, pore volume, and pore size of $Fe_3O_4$/rGO are evidently much lower than those of $MnO_2/Fe_3O_4$/rGO. $MnO_2$ layer forms on the $Fe_3O_4$/rGO surface different positions, thereby increasing surface area, pore volume, and pore size of the $MnO_2/Fe_3O_4$/rGO. Nevertheless, various groups introduced on the surface of GO provide numerous sorption sites, thereby increasing the sorption capacities of $MnO_2/Fe_3O_4$/rGO.

**Table 1.** The physical properties of $Fe_3O_4$/rGO and $MnO_2/Fe_3O_4$/rGO.

| characteristics | $Fe_3O_4$/rGO | $MnO_2/Fe_3O_4$/rGO |
|---|---|---|
| surface area ($m^2\ g^{-1}$) | 24.99 | 58.02 |
| pore volume ($cm^3\ g^{-1}$) | 0.067 | 0.343 |
| av pore radius (nm) | 9.37 | 24.19 |

Figure 5A shows photographs of $MnO_2/Fe_3O_4$/rGO nanocomposites dispersed in deionized water. $MnO_2/Fe_3O_4$/rGO is promptly separated from the dispersion by holding the samples close to a magnet, as shown in Figure 5B, indicating that it is possible to manipulate this material by an external magnetic field.

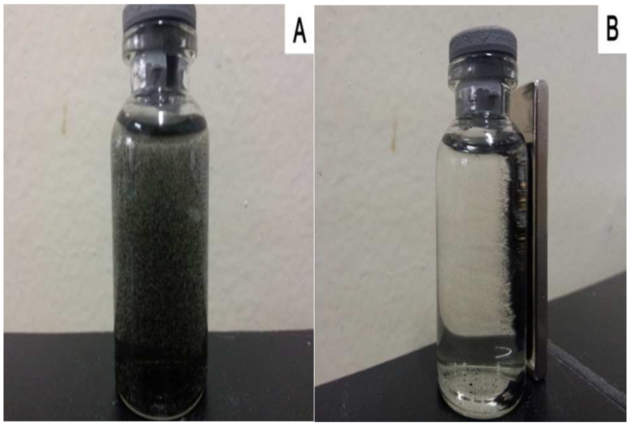

**Figure 5.** The inset demonstrates that 0.01 g/mL $MnO_2/Fe_3O_4$/rGO (A) can be dispersed in deionized water and separated from deionized water by a magnet (B).

## Adsorption Experiments

### Effect of solution pH

Solution pH is one of the most important factors that affect the adsorption process. The adsorption capacity of uranium (VI) versus pH is plotted in Figure 6 and shows that adsorption capacity increases with an increase in pH from 2.0 to 6.0, but decreases with further increase in pH from 6.0 to 12.0. Uranium (VI) uptake is obtained at a relatively broad range of pH (2 to 12) with an optimum pH at 6.0 and the minimum uranium (VI) uptake at pH 2.0. At lower pH, a high concentration of $H^+$ ion competes with uranyl ion for the binding sites on the sorbent surface,[37] resulting in a decreased adsorption of uranium (VI) at this pH. Along with the increase of pH, the surface of the adsorbent becomes negatively charged due to a deprotonation process, so that the Coulombic attraction between adsorbent and uranium (VI) probably strengthens the interaction between each other. However, at higher pH values, decrease in adsorption of uranium can be due to the formation of uranyl complexes such as $UO_2OH^+$, $(UO_2)_2(OH)_2^{2+}$ and $(UO_2)_3(OH)_5^+$.[38] Therefore, the optimum pH is 6.0 and all further experiments were conducted at an initial pH of 6.0.

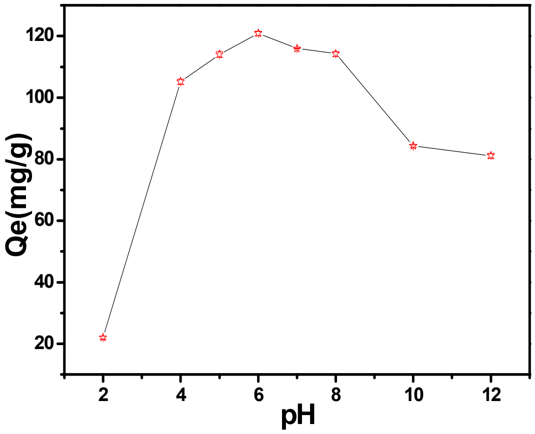

**Figure 6.** Effect of pH value on adsorption property of $MnO_2/Fe_3O_4$/rGO. pH 2.0-12.0; temperature 25 °C; amount of $MnO_2/Fe_3O_4$/rGO 0.02 g.

## Zeta Potential Measurements

The zeta potential of the $MnO_2/Fe_3O_4$/rGO covered with uranium (VI) and $MnO_2/Fe_3O_4$/rGO can provide valuable information on the surface forms of the adsorbates since the formation of the surface complexes will change the surface charge (Figure 7). Over the full pH range studied, $MnO_2/Fe_3O_4$/rGO had negative surface charge with very low the point of zero charge (PZC) values (3.9). After uranium (VI) loading, the ζ-potential values of $MnO_2/Fe_3O_4$/rGO shifted positively below pH 6. The positive shift in surface charge suggested that uranium (VI) was adsorbed as cationic or neutral innersphere surface complexes that could make the net surface charge less negative.[39] Above pH 6, $MnO_2/Fe_3O_4$/rGO materials was highly negatively charged and the impact of uranium (VI) sorption on their ζ-potentials became less pronounced.

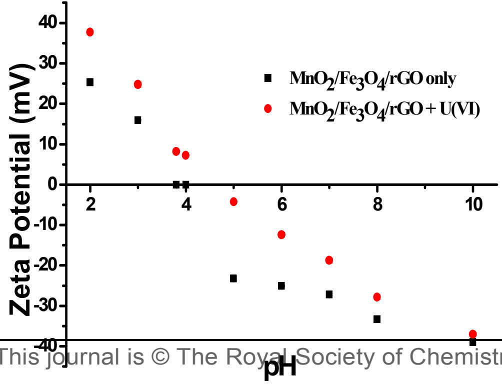

Figure 7. ζ-Potential of $MnO_2/Fe_3O_4$/rGO sample (0.01 mg/L) equilibrated with and without 50 mg/L total uranium (VI) at different pH values.

### Effect of adsorbent dose

Adsorbent dose is another factor that influences the adsorption equilibrium. To examine the effect of adsorbent dose on uranium (VI) removal, adsorption experiments were set up with various amounts of $MnO_2/Fe_3O_4$/rGO from 0.005 to 1.0 g. Figure 8 shows the effect of adsorbent dose on removal efficiency, adsorption capacity, and the theoretical maximum adsorption capacity of uranium (VI). From Figure 8 the removal efficiency of uranium (VI) increases rapidly with the increasing dosage of $MnO_2/Fe_3O_4$/rGO and then approaches equilibrium, while the adsorption capacity decreases. The increase of adsorption capacity is attributed to the availability of more adsorption sites. With increasing $MnO_2/Fe_3O_4$/rGO base content, the available sites on $MnO_2/Fe_3O_4$/rGO base surfaces increase and provide more sorption sites to adsorb uranium (VI) ions, thereby resulting in the increase of uranium (VI) ion sorption. From an economical point of view, the 0.02 g adsorbent dose is selected as the optimum dose.

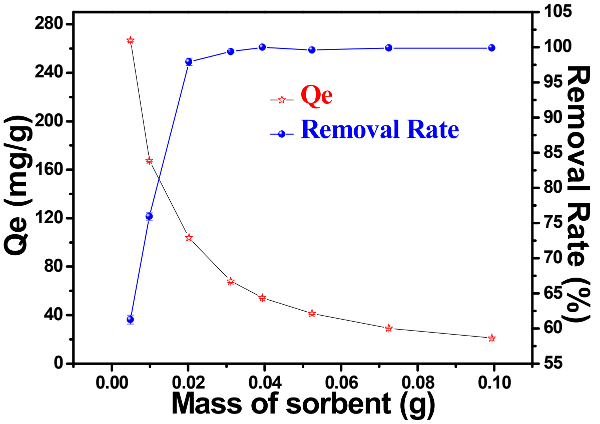

**Figure 8.** The effect of adsorbent dose on the uptake of uranium (VI) by $MnO_2/Fe_3O_4$/rGO. pH 6.0; temperature 25 °C; amount of $MnO_2/Fe_3O_4$/rGO 0.005-0.1 g.

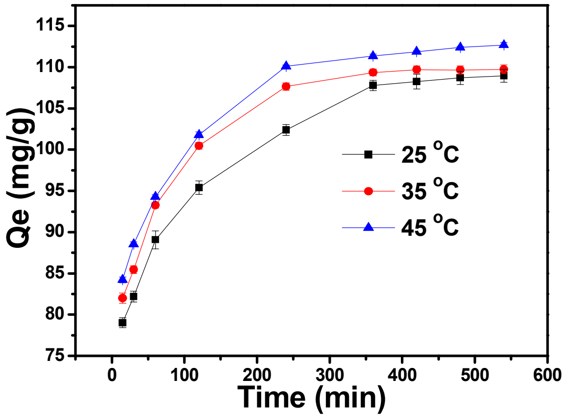

**Figure 9.** Effect of contact time on uranium (VI) adsorption. pH 6.0; temperature 25-45 °C; amount of $MnO_2/Fe_3O_4$/rGO 0.02 g.

### Effect of contact time and adsorption dynamics

The results of the effect of adsorption time on the adsorption capacity at different initial solution concentrations show that the removal of uranium (VI) increases with increasing contact time (Figure 9). In addition, the adsorption process reaches equilibrium with an initial uranium (VI) solution of 120 mg $L^{-1}$ and contact time of 360 min. Therefore, the contact time was set to 400 min in future experiments to ensure each adsorption equilibrium is achieved. As a result, a maximum equilibrium capacity of 110.6 mg $g^{-1}$ is obtained with an initial uranium (VI) solution of 120 mg $L^{-1}$.

Utilization of appropriate kinetic models can offer useful information for understanding the underlying sorption mechanisms. From this aspect, the experimental kinetic data of uranium (VI) sorption on $MnO_2/Fe_3O_4$/rGO were simulated by pseudo-first-order and pseudo-second-order models.[40–42] The pseudo-first-order kinetic model describes the sorption process based on sorbent capacity and can be written as:

$$\ln(q_e - q_t) = \ln(q_e) - k_1 t \tag{3}$$

The pseudo-second-order model considers the whole sorption process including external film diffusion, sorption, and internal particle diffusion, and can be written as:

$$\frac{t}{q_t} = \frac{1}{k^2 \cdot q_e^2} + \frac{t}{q_e} \tag{4}$$

where $q_e$ and $q_t$ are the sorption amounts of uranium (VI) (mg $L^{-1}$)at equilibrium time (h) and time $t$ (h), respectively; $k_1$ ($min^{-1}$) and $k_2$ (g $mg^{-1}$ $min^{-1}$) represent the kinetic rate constants of the pseudo-first-order and pseudo-second-order models, respectively. From the linear plot of ln($q_e$ -$q_t$) vs $t$ (Figure 10A), the $k_1$ and theoretical $q_e$ values ($q_{e,cal}$) of the pseudo-first-order model are obtained. And from the linear plot of $t/q_t$ vs $t$ (Figure 10B), the $k_2$ and $q_{e,cal}$ values of the pseudo-second-order model are obtained. The calculated kinetic parameters from both model fittings are shown in Table 2. Obviously, the correlation coefficient ($R^2$) of the pseudo-second-order model is higher than that of the pseudo-first-order model. Moreover, the $q_{e,cal}$ value for the pseudo-second-order model is nearer to the experimental value ($q_{e,exp}$). These results indicate that the kinetic data are simulated better by the pseudo-second-order model than the pseudo-first-order model. This phenomenon further implies that the dominant mechanism for uranium (VI) sorption on $MnO_2/Fe_3O_4$/rGO is chemisorption or strong surface complexation rather than mass transport.[43]

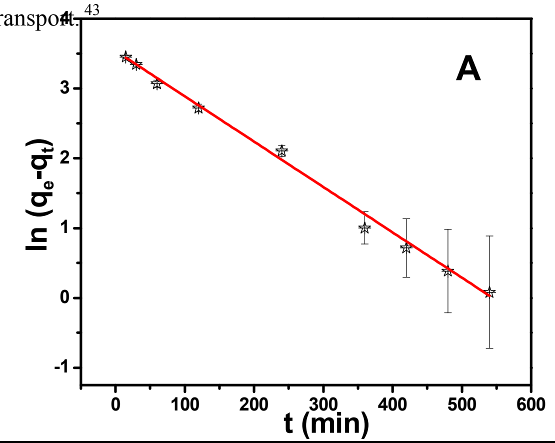

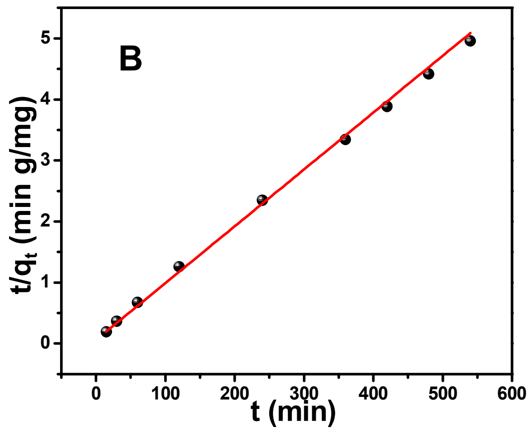

**Figure 10.** Pseudo-first-order (A), pseudo-second-order (B) plot for the removal of uranium (VI) by $MnO_2/Fe_3O_4/rGO$. pH 6.0; temperature 25 °C; amount of $MnO_2/Fe_3O_4/rGO$ 0.02 g.

**Table 2.** Pseudo-first-order and pseudo-second-order constants and values of $R^2$ for $MnO_2/Fe_3O_4/rGO$.

| Kinetic model | $T$ (°C) | $C_0$ (mg/L) | $Q_e^{exp}$ (mg/g) | $Q_e^{cal}$ (mg/g) | $k_1$(min$^{-1}$)/$k_2$ (g/mg·min) | $R^2$ |
|---|---|---|---|---|---|---|
| Pseudo-first order | 25 | 120 | 110.6 | 34.48 | 0.0065 | 0.9872 |
| Pseudo-second order | 25 | 120 | 110.6 | 110.8 | 0.0382 | 0.9969 |

## Effect of temperature and adsorption thermodynamics

The adsorption experiments at different temperatures were also performed to evaluate the influence of temperature (25-55 °C) (Figure 11). The results show that the adsorption of uranium (VI) is favored with an increase of temperature.

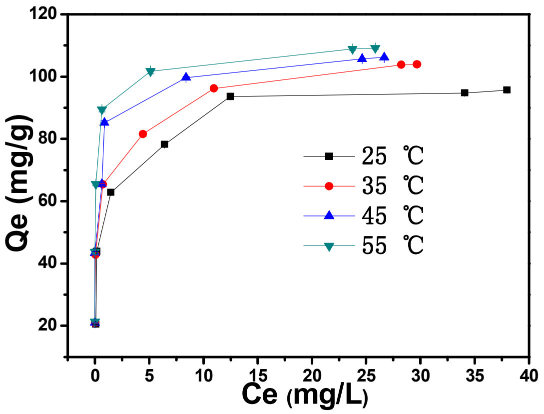

**Figure 11.** Adsorption isotherm of $MnO_2/Fe_3O_4/rGO$ for uranium (VI) at different temperatures. pH 6.0; temperature 25-55 °C; amount of $MnO_2/Fe_3O_4/rGO$ 0.02 g.

The thermodynamic property of the adsorbent-uranium (VI) system was calculated using the following equation: [44]

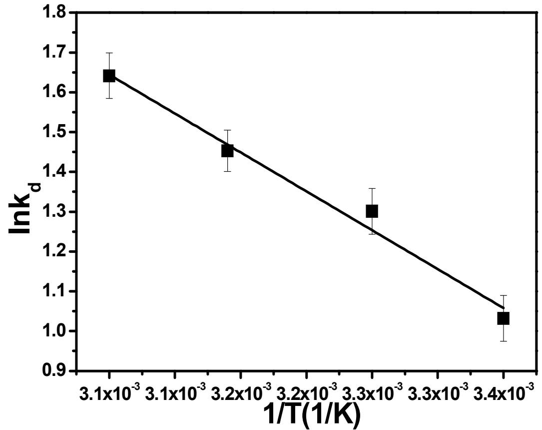

**Figure 12.** Relationship curve between ln $K_d$ and 1/T.

$$\ln K_d = \frac{\Delta S^0}{R} - \frac{\Delta H^0}{RT} \tag{5}$$

where $\Delta S°$ and $\Delta H°$ are the values of the entropy change and the enthalpy change during the process, $R$ (8.314 J mol$^{-1}$ K$^{-1}$) is the universal gas constant, $T$ (K) is the absolute temperature and $K_d$ is the distribution coefficient, which is expressed by: [45,46]

$$K_d = \frac{q_e}{C_e} \tag{6}$$

Furthermore, the value of the free energy change $\Delta G°$ is calculated by: [44]

$$\ln K_d = -\frac{\Delta G^0}{RT} \tag{7}$$

the values of $\Delta S°$, $\Delta H°$ and $\Delta G°$ were computed from the slope and intercept of plot between ln $K_d$ versus $1/T$, as shown in Figure 12. The calculated values of $\Delta S°$, $\Delta H°$ and $\Delta G°$ are shown in Table 3. A positive value of $\Delta S°$ indicates an increased randomness at the solid/liquid interface during the adsorption of uranium (VI) on $MnO_2/Fe_3O_4/rGO$. The positive value of $\Delta H°$ implies that the adsorption process was an endothermic reaction.[47] The negative values of $\Delta G°$ show the spontaneous nature of the process with uranium (VI) adsorbed onto the prepared adsorbent.[44, 48] With an increase of temperature, the values of $\Delta G°$ are more negative, which suggests that the equilibrium capacity increases. From the above results, the performance of uranium (VI) adsorbed on the as-prepared adsorbent is more favorable at higher temperatures.

**Table 3.** Thermodynamic parameters for uranium adsorption on $MnO_2/Fe_3O_4/rGO$.

| ΔH° (kJ mol$^{-1}$) | ΔS° (J mol$^{-1}$·K$^{-1}$) | ΔG° (kJ mol$^{-1}$) | | | |
|---|---|---|---|---|---|
| | | 25°C | 35 °C | 45 °C | 55 °C |
| 16.25 | 63.23 | -2.603 | -3.222 | -3.872 | -4.492 |

## Adsorption isotherms of uranium

The adsorption isotherms indicate the distribution of adsorbed molecules between the solid and liquid phase when the adsorption reaches an equilibrium. Isotherm studies provide information about the adsorption capacity of the adsorbent. To understand the adsorption behavior of the adsorbents, the equilibrium data were evaluated according to the Langmuir and Freundlich isotherm models.[49, 50]

The Langmuir isotherm assumes that the adsorbent surface is homogeneous, and a site can only by occupied by one pollutant molecule. The Langmuir isotherm is expressed by the following equation:

$$\frac{C_e}{q_e}=\frac{1}{b\cdot q_m}+\frac{C_e}{q_m} \qquad (8)$$

where $q_m$ is the maximum adsorption capacity (mg $g^{-1}$) and $b$ (L $mg^{-1}$) is the Langmuir binding constant, relating to the adsorption energy. Plotting $C_e/q_e$ versus $C_e$ gives a straight line with the slope equal to $1/q_m$ and intercept to $1/b\cdot q_m$. The theoretical plots from Langmuir isotherm and the experimental data for adsorption of uranium (VI) on adsorbent are shown in Figure 13.

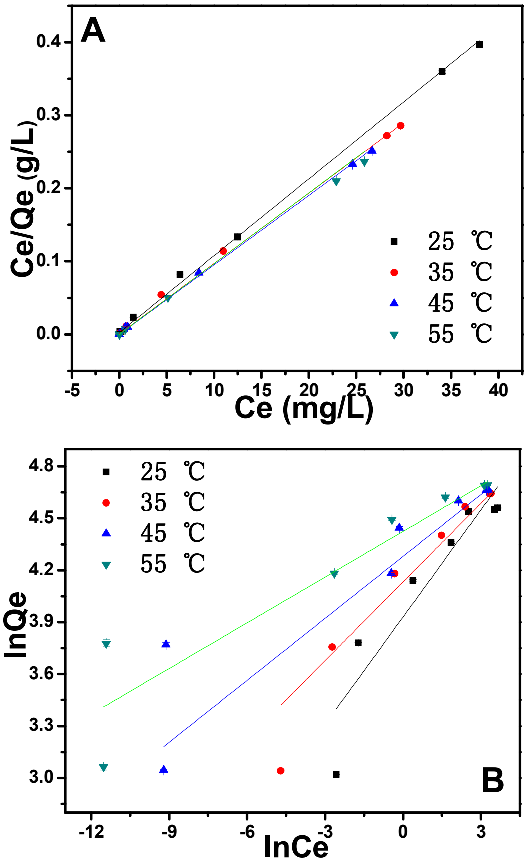

**Figure 13.** Comparison of the model fits of Langmuir(A) and Freundlich(B) for the removal of uranium (VI) by $MnO_2/Fe_3O_4$/rGO. pH 6.0; temperature 25-55 °C; amount of $MnO_2/Fe_3O_4$/rGO 0.02 g.

The Freundlich isotherm is expressed by an empirical equation, which is represented by: [51]

$$\ln q_e=\ln k+\frac{1}{n}\ln C_e \qquad (9)$$

where $k$ and $n$ are the Freundlich constants related to the sorption capacity and sorption intensity, respectively.

The linear plots of Langmuir and Freundlich equations representing uranium (VI) sorption are illustrated in Figure 13. The corresponding Langmuir and Freundlich parameters, along with the correlation coefficients, are reported in Table 4. As shown in Figure 13A, the Langmuir model appears to be the best fitting model for uranium(VI) sorption with a high correlated coefficient $R^2$ (0.99). According to the Langmuir isotherm, monolayer saturation capacity of $MnO_2/Fe_3O_4$/rGO is about 108.7 mg $g^{-1}$ for uranium (VI) at 55 °C.

**Table 4.** Isotherm constants and values of $R^2$ for $MnO_2/Fe_3O_4$/rGO.

| T(°C) | Langmuir isotherm | | | Freundlich isotherm | | |
|---|---|---|---|---|---|---|
| | $Q_m$(mg $g^{-1}$) | $b$(L $mg^{-1}$) | $R^2$ | $K$(L $g^{-1}$) | $n$ | $R^2$ |
| 25 | 95.24 | 4.2 | 0.9633 | 50.84 | 4.836 | 0.7572 |
| 35 | 103.1 | 16.05 | 0.9963 | 62.28 | 6.596 | 0.9784 |
| 45 | 105.3 | 3338 | 0.9927 | 72.14 | 8.382 | 0.9538 |
| 55 | 108.7 | 45390 | 0.9703 | 83.39 | 11.36 | 0.9028 |

## Removal Mechanism

The adsorption capacity of $MnO_2/Fe_3O_4$/rGO for uranium (VI) is more than 100 mg $g^{-1}$ in this study, which is higher than most of the previously reported values of other materials. This can be attributed to several reasons: first, the presence of functional groups (such as C-H, -OH, and -COOH) on the surface of $MnO_2/Fe_3O_4$/rGO assures the capture of metallic cations ($UO^{2+}$) by surface complexation and cation exchange mechanisms.[52] Secondly, $Fe_3O_4$, which is on the surface of $MnO_2/Fe_3O_4$/rGO, is not only the functional group for separation material from the aqueous phase, but also a kind of adsorptive group. According to previous literature,[53, 54] $Fe_3O_4$ adsorbs both negatively and positively charged species at various pH values. For $Fe_3O_4$, it attracts negative uranium (VI) species at low pH by electrostatic attraction, which is beneficial for a high adsorption of uranium (VI) for $MnO_2/Fe_3O_4$/rGO. Finally, the most important adsorption group is $MnO_2$; the surface groups of $MnO_2$ are amphoteric and function as an acid or a base. The oxide surface undergoes protonation and deprotonation in response to a change of solution pH.[55] Under different pH values, uranium (VI) can be absorbed by positively charged $MnO_2/Fe_3O_4$/rGO through electrostatic attraction, or the positively charged $MnO_2$ possibly involves an exchange reaction of $UO^{2+}$ with MnOH. Further studies are needed to more precisely characterize the detailed adsorption mechanism.

## Desorption and regeneration studies

The reusability of the $MnO_2/Fe_3O_4$/rGO for the adsorption of uranium (VI) is a crucial factor because better repeated availability of advanced adsorbents may reduce the overall cost of the adsorbent. Therefore, regeneration of $MnO_2/Fe_3O_4$/rGO was investigated to evaluate its potential application in removal and recovery of uranium (VI). As illustrated in Figure 6, the sorption amount of uranium (VI) is lower at lower pH values, implying that acid pickling is a possible approach for the regeneration of uranium (VI)-loaded $MnO_2/Fe_3O_4$/rGO.[56,57] Desorption experiments were carried out with HCl solutions at different concentrations; the percentage desorption of HCl concentrations of 0.005, 0.01, 0.02, 0.04 and 0.05 M are 82.14%, 83.05%, 85.42%, 90.88%, 89.76%, respectively. The best optimum concentration of HCl, therefore, was determined as 0.04 M in terms of economical process.

To assess the reusability of the adsorbent, regenerated $MnO_2/Fe_3O_4$/rGO was used for four consecutive cycles. After four consecutive sorption/desorption cycles, the adsorption efficiency of uranium (VI) slightly decreases from 92.58% to 85.46%, indicating that $MnO_2/Fe_3O_4$/rGO can be used as a good performance adsorbent applied in the field of uranium (VI) ion removal.

## Conclusions

$MnO_2/Fe_3O_4$/rGO was successfully prepared by a straightforward method. The $MnO_2/Fe_3O_4$/rGO was used as adsorbent for uranium (VI) ions from the aqueous solution. The sorption is strongly dependent on pH and the maximum adsorption capacity, calculated from the Langmuir isotherm model of the $MnO_2/Fe_3O_4$/rGO, was 108.7 mg $g^{-1}$ at 55 $^{o}$C. Thermodynamic data suggest that the sorption of uranium (VI) on $MnO_2/Fe_3O_4$/rGO is a spontaneous and endothermic process. In addition, uranium (VI)-loaded $MnO_2/Fe_3O_4$/rGO is easily separated from aqueous solutions by a magnet and efficiently renewed with HCl. The easy operation and fast and efficient sorption performance indicate that $MnO_2/Fe_3O_4$/rGO can be used as a highly effective material for the removal and recovery of uranium (VI) from contaminated wastewater and seawater.

## Acknowledgements

This work was supported by National Natural Science Foundation of China (21353003), Special Innovation Talents of Harbin Science and Technology (2013RFQXJ145), Fundamental Research Funds of the Central University (HEUCFZ), Natural Science Foundation of Heilongjiang Province (B201316), Program of International S&T Cooperation special project (2013DFA50480), and the fund for Transformation of Scientific and Technological Achievements of Harbin (2013DB4BG011), Research and Development of Industrial Technology Project of Jilin Province (JF2012C022-4)

## Notes and references

[a] *Key Laboratory of Superlight Material and Surface Technology, Ministry of Education, Harbin Engineering University, Harbin 150001, China. Tel. +86 451 8253 3026; fax: +86 451 8253 3026.*
*E-mail address: zhqw1888@sohu.com*

[b] *State Key Laboratory of Theoretical and Computational Chemistry, Institute of Theoretical Chemistry, Jilin University, Changchun 130023, China.*

[c] *Institute of Advanced Marine Materials, Harbin Engineering University, 150001, China.*

1. R. Han, W. Zou, Z. Zhang, J. Shi, J. Yang, J. Hazard. Mater. 2006, 137, 384-395.
2. L.M. Camacho, S.G. Deng, R.R. Parra, J. Hazard. Mater. 2010, 175, 393–398.
3. A. Mellah, S. Chegrouche, M. Barkat, Hydrometallurgy. 2007, 85, 163.
4. H. Singh, S.L. Mishra, R. Vijayalakshmi, Hydrometallurgy. 2004, 73, 63.
5. C.S.K. Raju, M.S.A. Subramanian, J. Hazard. Mater. 2007, 145,315.
6. A.M.S. John, R.W. Cattrall, S.D. Kolev, J. Membr. Sci. 2010, 364, 354.
7. G.H. Wang, J.S. Liu, X.G. Wang, Z.Y. Xie, N.S. Deng, J. Hazard. Mater. 2009, 168, 1053.
8. T.L. Prasad, P.K. Tewari, D. Sathiyamoorthy, Ind. Eng. Chem. Res. 2010, 49, 6559.
9. N. Kabay, M. Demircioglu, S. Yaylı, E. Gunay, M. Yuksel, M. Saglam, M. Streat, Ind. Eng. Chem. Res. 1998, 37, 1983.
10. L. Fan, C. Luo, M. Sun, H. Qiu, J. Mater. Chem. 2012, 22, 24577.
11. K. Lü, G. Zhao, X Wang, Chin. Sci. Bull. 2012, 57, 1223–1234.
12. R. Zacharia, H. Ulbricht, T. Hertel, Phys. Rev. B. 2004, 69, 155406.
13. Z. Wu, D. Wang, W. Ren, J. Zhao, G. Zhou, F. Li, H. Cheng, Adv. Funct. Mater. 2010, 20, 3595–3602.
14. J. Wang, T. Tsuzuki, B. Tang, X. Hou, L. Sun, X. Wang, ACS Appl. Mater. Interfaces. 2012, 4, 3084–3090.
15. S. Bai, X. Shen, X. Zhong, Y. Liu, G. Zhu, X. Xu, K. Chen, Carbon. 2012, 50, 2337–2346.
16. N. Li, M. Zheng, X. Chang, G. Ji, H. Lu, L. Xue, L. Pan, J. Cao, J. Solid State Chem. 2011, 184, 953–958.
17. Y. Ren, N. Yan, Q. Wen, Z. Fan, T. Wei, M. Zhang, J. Ma, Chem. Eng. J. 2011, 175, 1–7.
18. L. Hao, H. Song, L. Zhang, X. Wan, Y. Tang, Y. Lv, J. Colloid Interf. Sci. 2012, 369, 381–387.
19. B. Li, H. Cao, G. Yin, Y. Lu, J. Yin, J. Mater. Chem. 2011, 21, 10645–10648.
20. P. Wang, Q. Shi, Y. Shi, K.K.; Clark, G.D. Stucky, A.A. Keller, J. Am. Chem. Soc. 2009, 131, 182–188.
21. Z. Sun, L. Wang, P. Liu, S. Wang, B. Sun, D. Jiang, F. Xiao, Adv. Mater. 2006, 18, 1968–1971.
22. J. Hu, L. Zhong, W. Song, L. Wan, Adv. Mater. 2008, 20, 2977–2982.
23. V. Rocher, A. Bee, J.M. Siaugue, V. Cabuil, J. Hazard. Mater. 2010, 178, 434–439.
24. Y.M. Zhai, J.F. Zhai, M. Zhou, S.J. Dong, J. Mater. Chem. 2009, 19, 7030–7035.
25. C. Cunha, S. Panseri, D. Iannazzo, A. Piperno, A. Pistone, M. Fazio, A. Russo, M. Marcacci, S. Galvagno, Nanotechnology. 2012, 23, 465102.
26. A.H. Lu, E.L. Salabas, F. Schuth, Angew. Chem., Int. Ed. 2007, 46, 1222–1244.
27. N.A. Frey, S. Peng, K. Cheng, S.H. Sun, Chem. Soc. Rev. 2009, 38, 2532–2542
28. W.S. Hummers, R.E. Offeman, J. Am. Chem. Soc. 1958, 80, 1339.
29. S.B. Ma, K.Y. Ahn, E.S. Lee, K.H. Oh, K.B. Kim, Carbon. 2007, 45, 375-382.

30. Y.C. Si, E.T. Samulski, Chem. Mater. 2008, 20, 6792–6797.
31. X. Huang, C. Pan, X. Huang, Mater. Lett. 2007, 61, 934-936.
32. S.G. Wang, W.X. Gong, X.W. Liu, Y.W. Yao, B.Y. Gao, Q.Y. Yue, Sep. Purif. Technol. 2007, 58, 17–23.
33. B. Yang, Q. Gong, L. Zhao, H. Sun, N. Ren, J. Qin, J. Xu, H. Yang, Desalination. 2011, 278, 65-69.
34. H. Xia, M. Lai, L. Lu, J. Mater. Chem. 2010, 20, 6896−6902.
35. S. H. Sun, H. Zeng, D. B. Robinson, S. Raoux, P. M. Rice, S. X. Wang and G. X. Li, J. Am. Chem. Soc. 2004, 126, 273–279.
36. D.D. Shao, C.L. Chen, X.K.Wang, Chem. Eng. J. 2012, 144, 185−186.
37. J. Song, H. Kong, J. Jang, J. Colloid Interface Sci. 2011, 359, 505–511.
38. M. Sutton, S.R. Burastero, Chem. Res. Toxicol. 2004, 17, 1468.
39. M. Wazne, G. P. Korfiatis, X. G. Meng, Environ. Sci. Technol. 2003, 37 (16), 3619−3624.
40. Y.S. Ho, G. McKay, Water Res. 2000, 34, 735–742.
41. Y.S. Ho, G. McKay, Process Biochem. 1999, 34, 451–465.
42. Y.S. Ho, J. Hazard. Mater. 2006, 136, 681–689.
43. A. Kamari, W.S.W. Ngah, M.Y. Chong, M.L. Cheah, Desalination. 2009, 249, 1180–1189.
44. G. Moussavi, R. Khosravi, Chem. Eng. Res. Des. 2011, 89, 2182–2189.
45. W.T. Tsai, Y.M. Chang, C.W. Lai, C.C. Lo, J. Colloid Interface Sci. 2005, 289, 333–338.
46. M. Sprynskyy, B. Buszewski, A.P. Terzyk, J. Namiesnik, J. Colloid Interface Sci. 2006, 304, 21–28.
47. H. Teng, C. Hsieh, Ind. Eng. Chem. Res. 1998, 37, 3618–3624.
48. G. Crini, Dyes Pigments. 2008, 77, 415–426.
49. I. Langmuir, J. Am. Chem. Soc. 1918, 40, 1361–1403.
50. Freundlich, Z. Phys. Chem. 1906, 57, 385–470.
51. H.M.F. Freundlich, J. Phys. Chem. 1906, 57, 385–470.
52. J. Hu, C. Chen, X. Zhu, X. Wang, J. Hazard. Mater. 2009, 162, 1542-1550.
53. W. Jiang, M. Pelaez, D.D. Dionysiou, M.H. Entezari, D. Tsoutsou, K. O'Shea, Chem. Eng. J. 2013, 222, 527-533.
54. S.R. Chowdhury, E.K. Yanful, A.R. Pratt, J. Hazard. Mater. 2012, 235-236, 246-256.
55. R. Han, W. Zou, Z. Zhang, J. Shi, J. Yang, J. Hazard. Mater. 2006, 137, 384-395.
56. S.T. Yang, P.F. Zong, X.M. Ren, Q. Wang, X.K. Wang, ACS Appl. Mater. Interfaces. 2012, 4, 6890–6899.
57. G. Tian, J.X. Geng, Y.D. Jin, C.L. Wang, S.Q. Li, Z. Chen, H. Wang, Y.S. Zhao, S.J. Li, J. Hazard. Mater. 2011, 190, 442–450.

Table of Contents

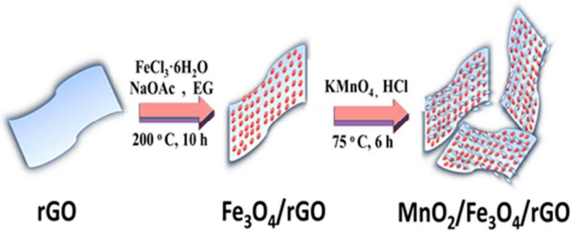

$MnO_2/Fe_3O_4$/rGO was prepared and exhibited fast and efficient sorption for uranium (VI).